AIP | Journal of Applied Physics

Experimental and theoretical correlation of very intense visible green photoluminescence in BaZrO3 powders

L. S. Cavalcante, V. M. Longo, M. Zampieri, J. W. Espinosa, P. S. Pizani et al.

Citation: J. Appl. Phys. **103**, 063527 (2008); doi: 10.1063/1.2901176
View online: http://dx.doi.org/10.1063/1.2901176
View Table of Contents: http://jap.aip.org/resource/1/JAPIAU/v103/i6
Published by the AIP Publishing LLC.

Experimental and theoretical correlation of very intense visible green photoluminescence in $BaZrO_3$ powders

L. S. Cavalcante,[1,a)] V. M. Longo,[1] M. Zampieri,[1] J. W. M. Espinosa,[1] P. S. Pizani,[1] J. R. Sambrano,[2] J. A. Varela,[2] E. Longo,[2] M. L. Simões,[3] and C. A. Paskocimas[4]
[1]*LIEC-DQ, PPGCEM, Universidade Federal de São Carlos, P.O. Box 676, 13565-905, São Carlos, SP, Brazil*
[2]*LIEC-IQ, Universidade Estadual Paulista, P.O. Box 473 e 355, 17033-360 e 14801-907, Bauru e Araraquara-SP, Brazil*
[3]*EMBRAPA Agricultural Instrumentation, P.O. Box 741, 13560-970, São Carlos-SP, Brazil*
[4]*Laboratório de Análise Térmica e Materiais, Departamento de Química, UFRN, P.O. Box 1662, 59072-970, Natal, RN, Brazil*

(Received 21 September 2007; accepted 28 January 2008; published online 31 March 2008)

Very intense visible green photoluminescence (PL) was observed at room temperature in structurally ordered-disordered $BaZrO_3$ powders. *Ab initio* calculations, ultraviolet-visible absorption spectroscopy, electron paramagnetic resonance, and PL were performed. Theoretical and experimental results showed that local defects in the cubic structure caused by $[ZrO_5 \cdot V_O^x]$ complex clusters, where $V_O^x = V_O^x$, $V_O^{\bullet}$, and $V_O^{\bullet\bullet}$, play an important role in the formation of hole-electron pairs, giving rise to a charge gradient in the structure which is responsible for PL emission. © *2008 American Institute of Physics*. [DOI: 10.1063/1.2901176]

I. INTRODUCTION

The recent development of materials with optical properties such as electroluminescence and photoluminescence (PL) can lead to new high performance optoelectronic devices.[1] Structurally disordered semiconductors can replace crystalline semiconductors, particularly when the cost is an important factor.[2] In particular, several theoretical and experimental studies have focused on perovskite titanates such as $CaTiO_3$,[3] $SrTiO_3$,[4] $BaTiO_3$,[5] and $PbTiO_3$ (Ref. 6) due to their excellent optical properties at room temperature. However, few studies have been reported on the photoluminescence of zirconates with visible emission regions,[7,8] especially those with visible light emission applied in high efficiency green/blue light-emitting diodes and high storage-capacity digital versatile disk (DVD) systems.

The short-wavelength region of the visible spectrum is attractive for application in higher density optical storage devices, as demonstrated in the latest generation of DVD players. Other advantages are the possibility of high-efficiency, long-lifetime, solid-state lighting using the green/blue wavelength to complement existing longer-wavelength sources for white lighting.[9] Hwang[10] showed that a radiative process from oxygen vacancies in the perovskite $SrTiO_3$ is able to induce the blue light emission. This author also argued that the obtained results by Kan *et al.*[11] opened a new way to investigate these phenomena in more deeply.

$BaZrO_3$ (BZO) is a material that presents several properties. In both doped and pure form, BZO is a very promising material for application in electroceramics and refractories owing the their thermal resistance and conductivity.[12] It can also be used as a protective agent against corrosion in the single growth of superconductors.[13,14] Moreover, the excellent thermomechanical properties[15] of this material are interesting for aerospace industries and correlated areas. This ceramic oxide can be used in solid oxide fuel cells and sensors that are proton conductors.[16] Yamanaka *et al.*[17] studied the thermochemical and thermophysical properties of several alkaline-earth perovskites, including the barium zirconate. The literature reports the study on the luminescence in crystalline BZO doped with europium,[18–20] but no reported experimental and theoretical studies on disordered barium zirconate.

In this way, we report in this paper the very intense green PL emission at room temperature in structurally ordered-disordered BZO powders prepared by the polymeric precursor method. We also show the importance on the correlation between the experimental results and theoretical calculations to understand the phenomenon of photoluminescence in BZO powders.

II. EXPERIMENT

BZO powders were synthesized by the polymeric precursor method. Barium nitrate, $Ba(NO_3)_2$ (99.9% Aldrich), zirconium *n*-propoxide, $[Zr(OC_3H_7)_4]$ (99.9% Aldrich), ethylene glycol, $C_2H_6O_2$ (99.5% synth), and citric acid, $C_6H_8O_7$ (99.5% synth) were used as raw materials. Zirconium citrate was formed by dissolving $Zr(OC_3H_7)_4$ in an aqueous solution of citric acid under constant stirring. The citrate solution was stirred at 85 °C to obtain a clear homogenous solution. $Ba(NO_3)_2$ was dissolved in solution and then added in a stoichiometric quantity to the Zr citrate. Ammonium hydroxide NH_4OH, 30% NH_3 Synth) was added to adjust the *p*H (*p*H 7–8) and to prevent the precipitation of barium citrate, which is favored in an acid solution.[21] After homogenization of Ba^{2+} cations, $C_2H_6O_2$ was added to promote a polyesterification reaction.[22] The citric acid/ethylene glycol ratio was fixed at 60:40. The resulting polymeric resin was then placed in a conventional furnace and heated to 350 °C for 4 h at a constant heating rate of 5 °C/min, causing it to pulverize

a)Electronic mail: laeciosc@bol.com.br.

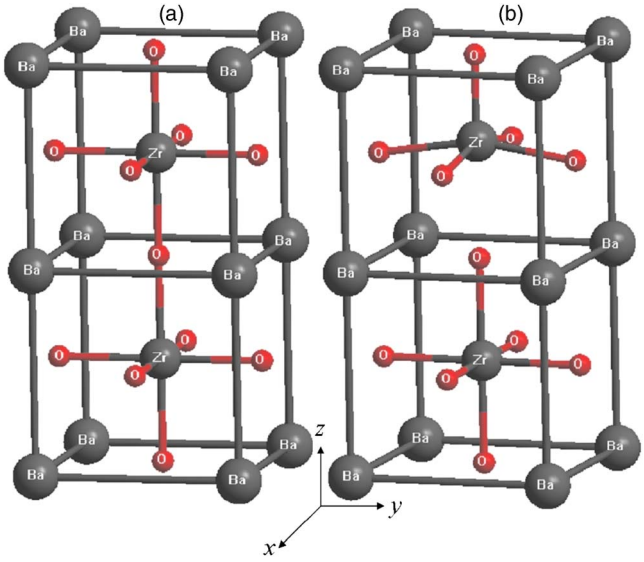

FIG. 1. (Color online) Supercell representation $1\times1\times2$ of the cubic BZO structure: (a) ordered BZO-*o* model and (b) disordered BZO-*d* model.

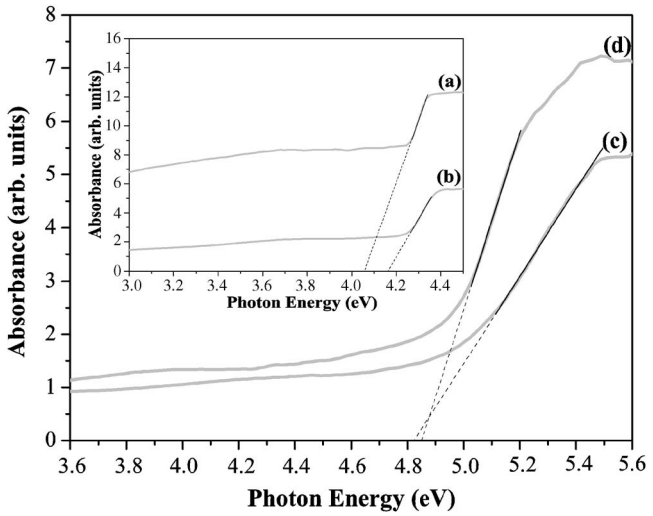

FIG. 2. UV-vis absorbance spectra of BZO powders annealed at (a) 400, (b) 450, (d) 500, and (d) 700 °C for 2 h under oxygen atmosphere.

and decomposing the organic part of the citric acid and ethylene glycol. These inorganic amorphous or disordered powders were annealed in a tube furnace with an oxygen atmosphere for 2 h at 400, 450, 500, and 700 °C, using a constant heating rate of 1 °C/min.

Ultraviolet-visible (UV-vis) absorption spectra of optical absorbance on disordered and ordered BZO powders were recorded using a Cary 5G spectrophotometer. Electron paramagnetic resonance (EPR) spectra were recorded on a Bruker EMX-300 spectrometer operating in the *X* band (9 GHz) and with a microwave power of 2 mW; amplitude modulation 1 G, time constant of 2.56 ms, conversion time 10.24 ms, and modulation frequency of 100 kHz. The *g* factor was referenced with respect to $MgO:Cr^{3+}$ ($g=1.9797$) as the external standard. The spectra were evaluated using the SIMFONIA program. The analysis involved at least 16 sweeps per determination. PL spectra were taken with a U-1000 Jobin-Yvon double monochromator coupled to a cooled GaAs photomultiplier and a conventional photon counting system. The 488.0 nm exciting wavelength of an argon ion laser was used, with the laser's maximum output power kept at 25 mW. A cylindrical lens was used to prevent the sample from overheating. The slit width used was 100 μm. All the measurements were taken at room temperature.

III. COMPUTATIONAL METHODS AND PERIODIC MODELS

Periodic density functional theory calculations with Becke's three-parameter hybrid nonlocal exchange functional[23] combined with the Lee–Yang–Parr gradient-corrected correlation functional[24] were made with the CRYSTAL03 computer code.[25] The functional used in this work yielded results comparable to more sophisticated correlated calculations or perturbation models. In fact, we have already employed this functional in studies of the electronic and structural properties of $BaTiO_3$ (Ref. 26) and $Pb_{1-x}Ca_xTiO_3$.[27] The atomic centers have been described by all electron basis sets 9763-311(d631)G, 976-31(d62)G^*, and 6-31G^* for Ba, Zr end O atoms, respectively, and can be found on the website.[28,29] The band structures were obtained along the appropriate high-symmetry paths of the Brillouin zone.

IV. RESULTS AND DISCUSSION

BZO presented a cubic perovskite-type structure in crystalline form with a space group $Pm\bar{3}m$. The obtained experimental value of the lattice constant a of BZO crystalline phase was 4.186 Å. The lattice parameters were calculated using the least square refinement of the UNITCELL-97 program.[30] As a first step, the lattice parameter was subjected to an optimization procedure, yielding a value of 4.262 Å. Different external algorithms have been tested to yield similar results, and the less computationally demanding Nelder–Mead (Simplex) method[31] has been employed. From this optimized structure, we built a $1\times1\times2$ supercell as a periodic model to represent the ordered BZO-*o* model, [see Fig. 1(a)]. This ordered model can be designed as $[ZrO_6]$–$[ZrO_6]$, since each Zr atom is surrounded by six O atoms. We assumed that before the powder became completely crystallized, i.e., before the heat treatment reached 700 °C, the structure was composed of an aleatory mixture of ZrO_6 octahedra linked by Ba^{2+} ions. The disordered BZO-*d* model is formed by the displacement of one Zr atom in the [001] direction. This displacement is the simplest way to represent the two environments of Zr, $[ZrO_5\cdot V_O^x]$ complex clusters, where $V_O^x = V_O^x$, $V_O^{\bullet}$, and $V_O^{\bullet\bullet}$ square-base pyramid, and $[ZrO_6]$ octahedron. Therefore, the BZO-*d* structure can be designed as $[ZrO_5\cdot V_O^x]$–$[ZrO_6]$ [see Fig. 1(b)].

This assumption was based on our X-ray absorption near-edge structure results of the crystallization process of $SrTiO_3$,[4] $PbTiO_3$,[6] and $CaTiO_3$,[32] which indicated the coexistence of the two types of environments for the titanium, namely, fivefold titanium coordination ($[TiO_5]$ square-base pyramid) and sixfold titanium coordination ($[TiO_6]$ octahedron). This slight order degree on structurally disordered ma-

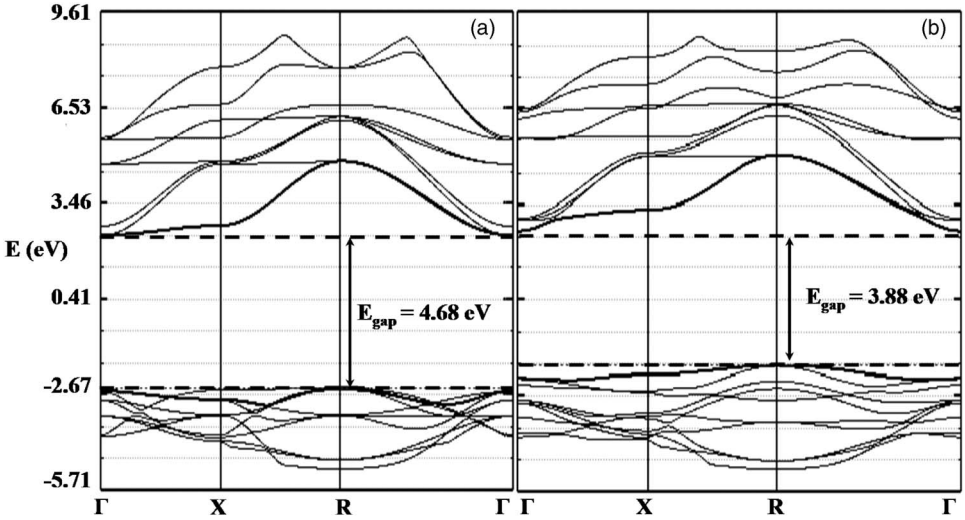

FIG. 3. Band structure of (a) BZO-*o* and (b) BZO-*d* models.

terials was expected, since two or more atoms arranged are close to each other in a stable configuration, which have some order degree due of the existence of a minimum potential energy. Furthermore, it is well known that the details of the band structure of a periodic system are determined mainly by the potential within the unit cell rather than by the long-range periodicity. This means that any perturbation of the symmetry in the unit cell will affect the electronic structure.

Our purpose with this BZO-*d* model is to provide a simple scheme to help shed light on the effects of structural deformation on the electronic structure without completely suppressing the geometry of the cell, which is useful for periodic calculations. Using the same kind of distorted model, we have explained the PL of various perovskite titanates[33,34], zirconate titanates,[35,36] and tungstates.[37,38]

Figure 2 shows the UV-vis absorption spectra of BZO powders annealed at 400, 450, 500, and 700 °C for 2 h in an oxygen atmosphere.

The exponential optical absorption edge and the optical band gap are controlled by the structural order-disorder degree on the lattice of BZO powders. The increase in the band gap can be ascribed to the reduction of defects in the lattice, which decrease the intermediary energy levels in the band gap region of disordered BZO powders. The powders annealed at 400, 450, and 500 °C presented a similar absorption behavior as in amorphous semiconductors, such as silicon and insulators [see Figs. 2(a)–2(c)]. Therefore, the BZO powders annealed at 700 °C showed a typical band in the high energy region of the absorbance curve for ordered or crystalline materials [see Fig. 2(d)]. In the disordered BZO powders, the absorbance measurements suggest a nonuniform on band gap structure with the presence of localized states. The optical band gap energy is related to the absorbance and to the photon energy, according to Wood and Tauc[39] as shown in

$$h\nu\alpha \propto (h\nu - E_g^{\text{opt}})^2, \tag{1}$$

where α is the absorbance, h is the Planck constant, ν is the frequency, and E_g^{opt} is the optical band gap.

Figure 3 shows the calculated band structures of the BZO-*o* and BZO-*d* models.

For the BZO-*o* model [see Fig. 3(a)], the calculations showed a band gap of 4.68 eV, which is very close to the experimental band gap value of 4.85 eV for the crystalline powder [see Fig. 2(f)]. For the BZO-*d* model [see Fig. 3(b)], the theoretical band gap is 3.88 eV after a displacement of 0.40 Å, which is comparable with the experimental value of 4.06 eV obtained for disordered powders annealed at 400 °C for 2 h [see Fig. 2(a)]. The gap between *R* in the valence band (VB) and Γ in the conduction band (CB) is indirect in the BZO-*o* and BZO-*d* models. These results with corroborate the interpretation that the band gap is controlled by the structural order-disorder degree in the BZO lattice (see Table I) with are in agreement with our previous studies of $BaTiO_3$ (BTO).[40] *Ab initio* calculations showed that ZrO_6 octahedra were more distorted than TiO_6 octahedra in BTO-BZO, as we reported in a subsequent paper.[41]

The theoretical and experimental optical gap values obtained from UV-vis spectroscopy are summarized in Table I.

The displacement of Zr atoms in the [001] direction allows the formation of intermediate levels in the region of band gap energy, leading to additional energy levels in the band gap of disordered BZO powders. The agreement between the experimental and theoretical results confirms the consistency of the disordered model.

To identify the predominant orbitals involved in localized states in that are observed on the disordered structure, the electronic structure was analyzed in terms of density of states (DOS).

The calculated total and atom-resolved projected DOS for BZO-*o* and BZO-*d* models are shown in Figs. 4(a) and

TABLE I. Experimental $Eg_{(expt)}$ gap energies in axis-*x* and theoretical $Eg_{(theor)}$ gap energies in the [001] direction of BZO powders.

$Temperature_{(expt)}$ (°C)	700	500	⋯	450	⋯	400	⋯	⋯
$Eg_{(expt)}$ (eV)	4.85	4.82	⋯	4.16	⋯	4.06	⋯	⋯
Displacement (Å)	0.00	0.10	0.20	0.30	0.31	0.32	0.35	0.40
$Eg_{(theor)}$ (eV)	4.68	4.58	4.36	4.12	4.10	4.07	4.00	3.88

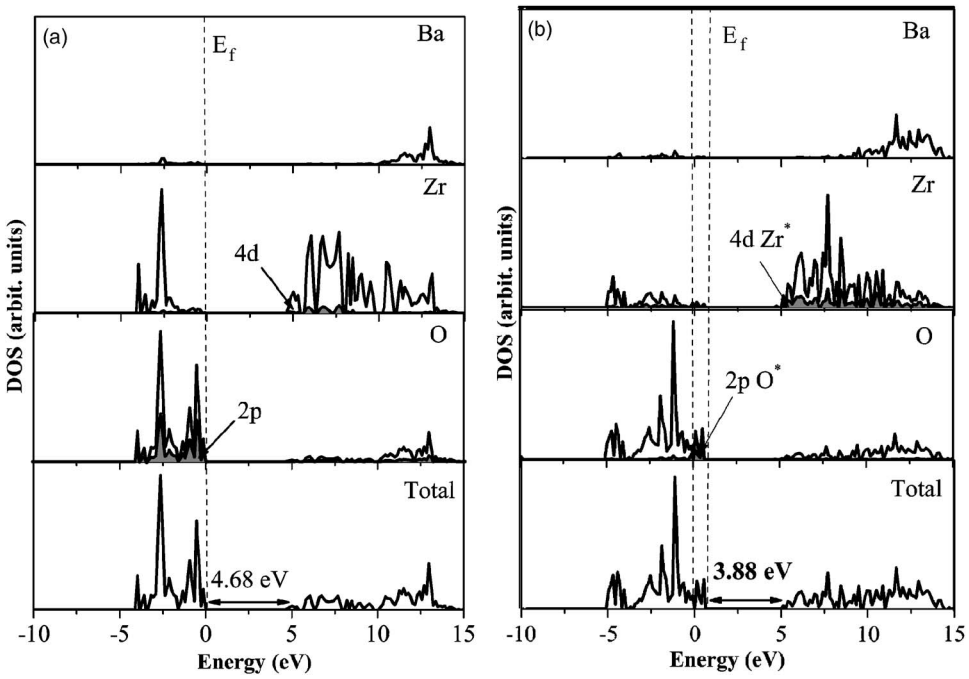

FIG. 4. Total and atom-projected density of states for the (a) BZO-*o* and BZO-*d* models.

4(b), ranging from −10 eV below the top of the VB to 15 eV above the CB. The zero of energy is taken at the top of the last occupied level (Fermi energy=E_F).

In the case of BZO-*o*, the upper VB is composed predominately of the O (2*p*) states, equally distributed on the six oxygens of the structure in Fig. 4(a). In the case of the BZO-*d* presented in Fig. 4(b), although the VB is also composed of the O (2*p*) states, the upper part, i.e., the new states have a strong oxygen character, the oxygen atom (O*) that loses the connection with Zr [Fig. 1(a)]. The CB clearly consists of the Zr (4*d*) states in both cases. The Zr–O covalent bond creates a limited Zr (4*d*) contribution in the O (2*p*) region, as well as a weak O (2*p*) contribution to the Zr* (4*d*) area. The Ba atoms states are found between 10 and 15 eV in the case of BZO-*o* and more dispersed in the case of BZO-*d*. These levels are weakly hybridized with the oxygen levels. It was calculated the atom-resolved projected DOS area of zirconium and oxygen in BZO-*o* and BZO-*d* models. Only the top of VB ranging from −5 eV to the Fermi energy was evaluated. The *ab initio* results indicated that the bonding character of the Zr and O in the BZO-*o* model is 7.5% and in the BZO-*d* model is 7.1%. The BZO-*o* structure is slightly more covalent than BZO-*d* structure.

Figure 5 shows the *X*-band EPR powder spectra of the BZO powders heat treated at 400, 450, 500, and 700 °C and recorded at room temperature.

The BZO powders annealed at 400 °C for 2 h presented an intense and asymmetric signal of the spin Hamiltonian at room temperature [see Fig. 5(a)]. In the literature, this signal is related with singly ionized oxygen vacancies ($V_O^{\bullet}$) and vacancy-related defects,[42–44] where the single symmetrical peak (*g*) presents some variations of 1.9560–2.0030. We believe that the changes in *g* values are related to differences in the preparation method, chemical environment, and heat treatment conditions. Matta *et al.*[45] used EPR measurements to verify the phase transformation from tetragonal to monoclinic zirconia and observed a signal ($g=2.0018$), which was attributed to trapped single electrons located in oxygen vacancies of ZrO_2. Lin *et al.*[46] reported that the EPR band at $g=1.9800$ is oxygen vacancy related. Thus, in the disordered structure, these $V_O^{\bullet}$ are linked to ZrO_5 clusters, called $[ZrO_5 \cdot V_O^{\bullet}]$ oxygen complex clusters. It is well known that electrons determine the transport properties, e.g., electrical conductivity, but no role-related phenomena have been observed. This indicates that the holes are trapped around crystal defects. The BZO powders annealed at 450 and 500 °C for 2 h showed a combination of structural defects, with oxygen vacancies responsible for the permanence of an asymmetric signal [see Figs. 5(b) and 5(c)]. Increasing the annealing heat promoted the elimination of $V_O^{\bullet}$ linked to $[ZrO_5]$ in BZO powder, causing the asymmetric signal in the EPR spectra to disappear [see Fig. 5(d)].

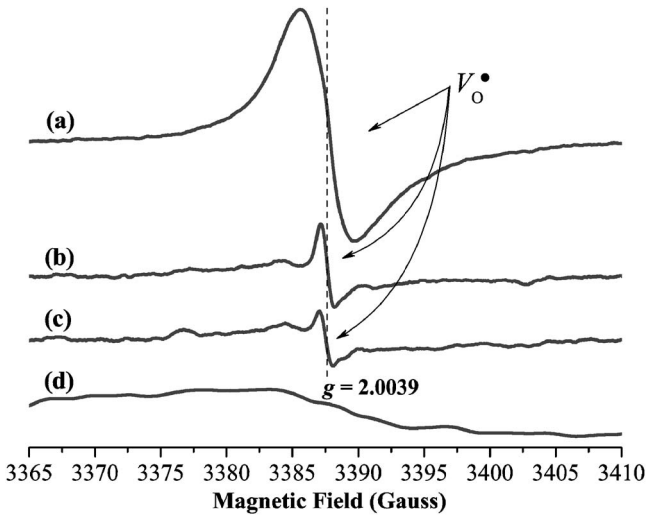

FIG. 5. *X*-band EPR measurements at room temperature for BZO powders after annealed at (a) 400, (b) 450, (c) 500, and (d) 700 °C for 2 h under oxygen atmosphere.

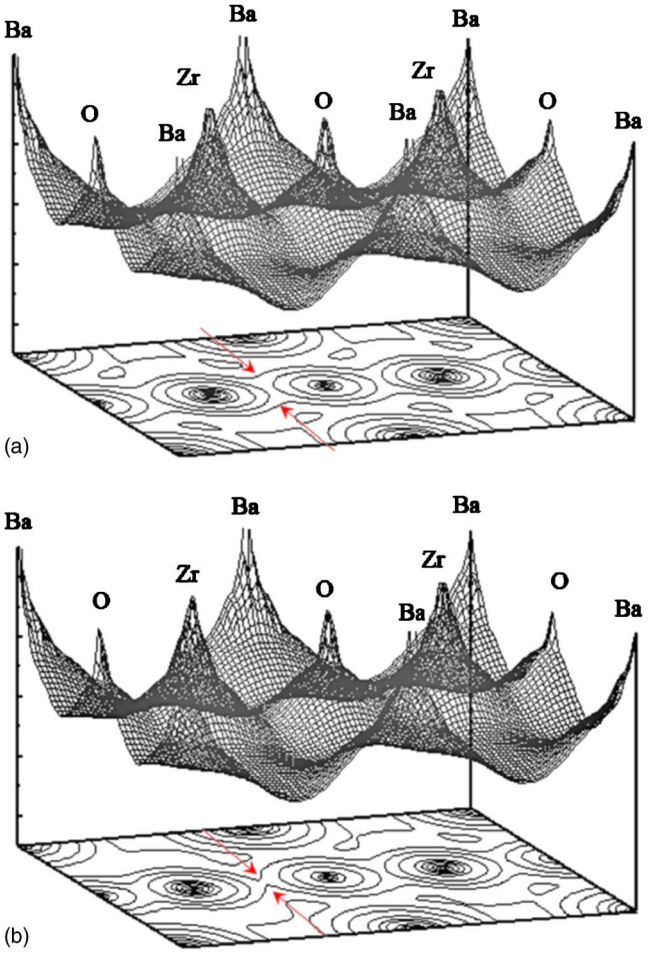

FIG. 6. (Color online) Contour and surface plots of the electronic density of charge calculated in the (110) plane for (a) BZO-c model and (b) BZO-*d* model. The arrows indicate the differences observed in surface plots.

The EPR spectra suggest that greater annealing heat reduces the singly ionized oxygen vacancies in disordered BZO powders, creating electron-captured oxygen vacancies, according to the following equations:

$$[ZrO_6]^x + [ZrO_5 \cdot V_O^x] \rightarrow [ZrO_6]' + [ZrO_5 \cdot V_O^{\cdot}] \quad (2)$$

$$[ZrO_6]^x + [ZrO_5 \cdot V_O^{\cdot}] \rightarrow [ZrO_6]' + [ZrO_5 \cdot V_O^{\cdot\cdot}] \quad (3)$$

$$[ZrO_5 \cdot V_O^{\cdot\cdot}] + \frac{1}{2}O_2 \rightarrow [ZrO_6] \quad (4)$$

In this structure, the $[ZrO_5 \cdot V_O^x]$ oxygen complex clusters are donor candidates, $[ZrO_6]^x$ clusters are acceptor candidates and $[ZrO_5 \cdot V_O^{\cdot}]$ are donor-acceptor candidates, where $[ZrO_5 \cdot V_O^x]$ presenting two paired electrons $\underline{\uparrow\downarrow}$, $[ZrO_5 \cdot V_O^{\cdot}]$ one unpaired electron $\underline{\uparrow}$ and $[ZrO_5 \cdot V_O^{\cdot\cdot}]$ no unpaired electron__. Thus, the EPR technique only detects species that possess unpaired electrons—in this case, $[ZrO_5 \cdot V_O^{\cdot}]$ oxygen complex clusters. We assume that charge redistribution may lead to electron-hole recombination of localized excitons $[ZrO_6]'$ with $[ZrO_5 \cdot V_O^{\cdot}]$.

Figure 6 exhibits the surface and contours plots of the charge density for the two models taken in the (110) plane containing Ba, Zr, and O atoms.

Figure 6(a) illustrates the electronic density maps in the (110) diagonal plane BZO-*o*. The diagonal cutting plane passes through of the Ba, Zr, and Ba atoms that are perpendicular to the square-base plane. This figure illustrates the covalent character of the interaction of the Zr atoms with the O atoms from the hybridization between the $2p$ atomic orbital of the O atoms and the $4d$ atomic orbitals of the Zr atoms. However, this covalent character as discussed in DOS projected states are weak. This behavior is represented by the homogeneous distributions of the contour lines. The formal charge between the symmetric $[ZrO_6]$–$[ZrO_6]$ clusters for the ordered structure presents zero value. Figure 6(b) shows electron density maps involving the Zr, Ba, and O atoms for BZO–*d* model. An inhomogeneous distribution is visualized by contour lines which represent the decrease in the interaction between the Zr–O atoms due to the breaking of these bonds. This charge gradient and the presence of the localized states provide a good condition for the trapping of electrons and holes. The charge transfer occurring from $[ZrO_5]$ to $[ZrO_6]$ clusters creates electron and hole polarons that can be designed as Jahn–Teller bipolarons. We have observed $(V_O^{\cdot})$ species by means of electron paramagnetic resonance measurements that possibly are linked to $[ZrO_5]$ clusters. The disordered structure presents a structural asymmetry that leads to a nonzero difference in formal charge between the clusters, suggesting the presence of polarization in this system.[47]

From earlier studies on perovskite titanates, we know that the network-formed clusters such as TiO_6 or TiO_5 clusters[48] are the first to be built during the crystallization process, as already discussed. Based on this proposal, we assume that before the heat treatment reaches 700 °C, the structure is composed of an aleatory mixture of ZrO_5 and ZrO_6 linked by barium ions. These ionic materials are stable because of short-range and long-range repulsions between adjacent electron clouds. The existence or absence of order or disorder is determined by the balance between these short-range and long-range repulsions, which favor the ordered or disordered structure, which might stabilize the noncrystalline, intermediate crystalline, or crystalline structure.[49] Even in disordered structures, the short-range repulsions predominate ($[ZrO_5 \cdot V_O^{\cdot}] \gg [ZrO_6]$), resulting in a random disorder. Because of the electric dipolar interaction, which, in this case, is a long-range interaction, the effective field approximation can be applied to a model system in which a dielectrically soft local atomic configuration can be identified, albeit possibly distorted in the glassy phase (noncrystalline). This disorder is produced by clusters of different coordinations ($[ZrO_6]$ and $[ZrO_5]$), forming nano-microentities whose size and order are determined by their temperature dependence. As the temperature increases, the stabilization forces associated with the polarization of the clusters as they are displaced become stronger than the short-range repulsive cluster-cluster interactions and the stable intermediate phase.

In our model, the wide-band model,[38] the most important events occur before excitation, i.e., before the photon arrives. The short and intermediate-range structural defects generate localized states in the band gap and inhomogeneous charge distribution in the cell, thus allowing for the trapping of elec-

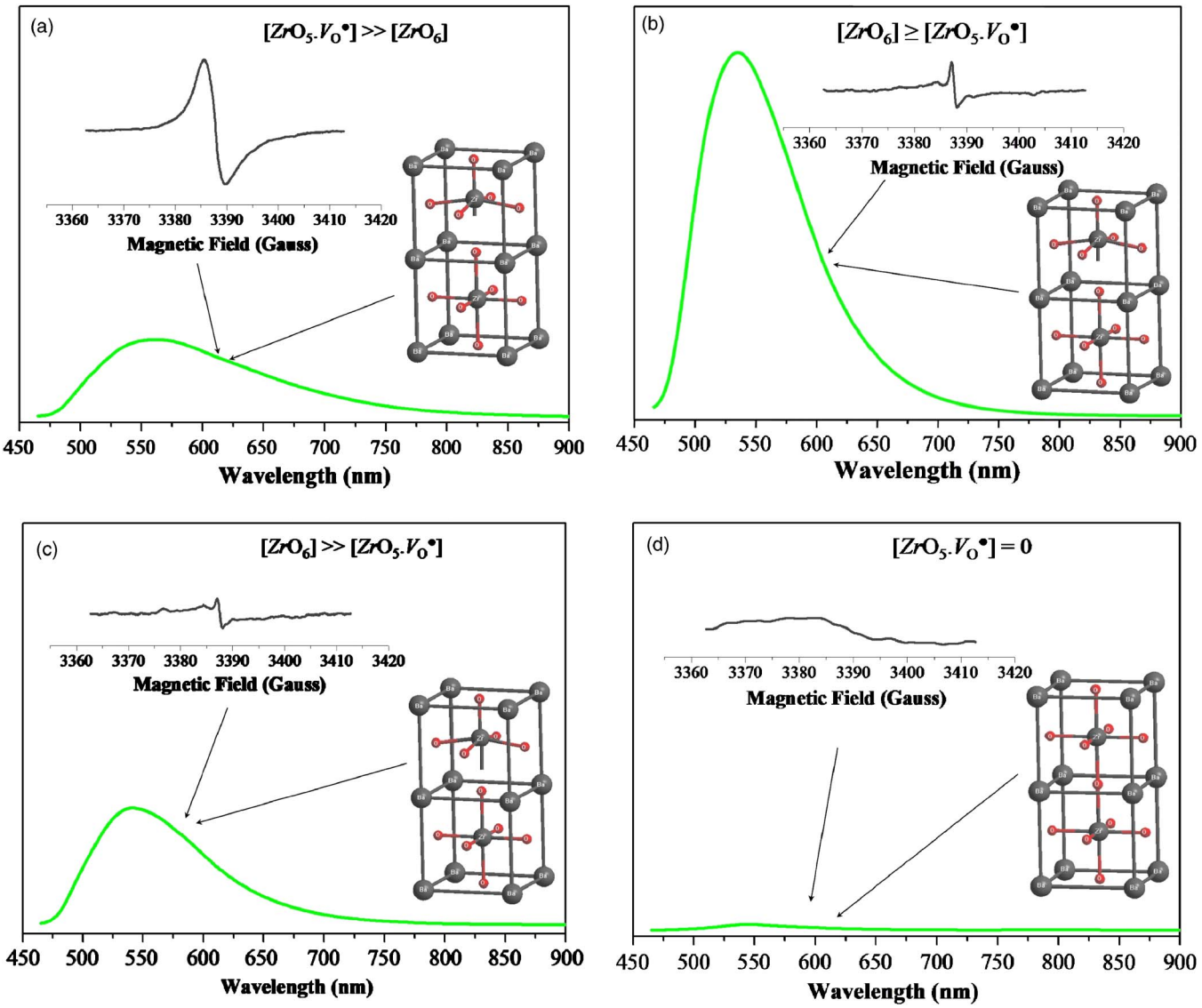

FIG. 7. (Color online) PL emission spectra of BZO powders annealed at (a) 400, (b) 450, (c) 500, and (d) 700 °C for 2 h under oxygen atmosphere. The inset shows correlation of EPR spectra and BZO-*d* and BZO-*o* models with PL behavior.

trons. The lower CB is mainly due to the 4*d* orbitals of the zirconium atoms. The levels responsible for the reduction of the band gap are mainly due to the oxygens of 2*p* orbitals in the VB, which are destabilized by the breaking of the Zr–O bond. The localized levels are energetically distributed so that various energies are able to excite the trapped electrons. After excitation of the photon describes the recombination process in which an electron of the CB loses its energy and reoccupies the energy levels of an electron (e') hole ($h^{\bullet}$) in the VB, the recombination and decay process follows the many valid hypotheses presented in the literature.[50,51]

Figure 7 shows the PL spectra recorded at room temperature for the BZO powders annealed at 400, 450, 500, and 700 °C for 2 h in an oxygen atmosphere.

The very intense green PL with maximum emission at ≅535 nm is associated with the structural order-disorder degree or defects in the BZO lattice after excited with a 488 nm excitation line. The emission band profile is a typical multiphonon process, i.e., a system in which the relaxation occurs by several paths, involving the participation of numerous levels within the perovskite band gap and self-trapping of electrons and charge transference in complex clusters.[52] Increasing the heat treatment temperature leads to the elimination of the EPR asymmetric signal, as illustrated in the inset [Figs. 7(a)–7(d)]. The correlation effect and models were used to illustrate the formation of $[ZrO_6]$–$[ZrO_6]$ clusters and reduction of the PL emission. We believe that the formation of holes ($h^{\bullet}$)/electrons (e') in the BZO lattice is very important for intense green PL emission.

Another way to explain the phenomenon of PL is associated with the low PL emission of disordered powder with a greater presence of complex clusters $[ZrO_5 \cdot V_O^{\bullet}]$ than of $[ZrO_6]$ clusters [see Fig. 7(a)]. The maximum PL emission is related to the structural order-disorder and the simultaneous presence of the $h^{\bullet}/e'$ pair in the BZO powder, a behavior that is attributed to the presence of complex clusters $[ZrO_6] \geqslant [ZrO_5 \cdot V_O^{\bullet}]$ [see Fig. 7(b)]. PL emission decreases due to the increase on structural order and reduction of complex clusters in $[ZrO_5 \cdot V_O^{\bullet}]$ the lattice [see Fig. 7(c)]. High

annealing temperatures increase the structural organization of the lattice, according to the following equation: $[ZrO_5 \cdot V_O^{\bullet\bullet}] + \frac{1}{2}O_2 \rightarrow [ZrO_6]$ [see Fig. 7(d)] and the vanish of PL emission. Our EPR measurements confirmed the presence of $V_O^{\bullet}$ species. In our theoretical calculations, we consider punctual defects in the BZO lattice.

V. CONCLUSIONS

In conclusion, BZO powders synthesized by the polymeric precursor method present very intense green PL emission centered at around 535 nm. The experimental results of EPR measurements showed the presence of defects in the lattice resulting from inherent defects produced by $V_O^{\bullet}$ oxygen vacancies linked to $[ZrO_5]$ clusters. Our calculations indicate that localized states generated in the band gap reduce the gap energies. As the structural order increases, the gap energy increases. These observations confirmed the fact that PL emission at room temperature may be related to the structural order-disorder degree in the BZO lattice, which is controlled by $[ZrO_5 \cdot V_O^{\bullet}]$ and $[ZrO_6]$ clusters. The decrease of gap energy is due to the localized levels in the band gap together with charge discontinuities induced by local disorder, favor the trapping of e' and $h^{\bullet}$ during the excitation process, leading to photoluminescent emission. First principles calculations revealed that the main character of the localized levels in the upper VB are the $2p$ orbitals of oxygens (O^*), which lose their connection with the displaced Zr atoms. The results showed that theoretical models can be combined with the experimental data to explain the very intense green PL emission at room temperature and that the structural ordered-disordered in lattice, promote to necessary conditions to observation of this physical property.

ACKNOWLEDGMENTS

The authors gratefully acknowledge the agencies CAPES, FAPESP, and CNPq.

[1]M. Anicete-Santos, F. C. Picon, M. T. Escote, E. R. Leite, P. S. Pizani, J. A. Varela, and E. Longo, Appl. Phys. Lett. **88**, 211913 (2006).
[2]R. C. Lima, M. Anicete-Santos, E. Orhan, M. A. M. A. Maurera, A. G. Souza, P. S. Pizani, E. R. Leite, J. A. Varela, and E. Longo, J. Lumin. **126**, 741 (2007).
[3]F. M. Pontes, C. D. Pinheiro, E. Longo, E. R. Leite, S. R. de Lazaro, J. A. Varela, P. S. Pizani, T. M. Boschi, and F. Lanciotti, Mater. Chem. Phys. **78**, 227 (2003).
[4]F. M. Pontes, E. Longo, E. R. Leite, E. J. H. Lee, J. A. Varela, P. S. Pizani, C. E. M. Campos, F. Lanciotti, and C. D. Pinheiro, Mater. Chem. Phys. **77**, 598 (2003).
[5]F. M. Pontes, C. D. Pinheiro, E. Longo, E. R. Leite, S. R. de Lazaro, R. Magnani, P. S. Pizani, T. M. Boschi, and F. Lanciotti, J. Lumin. **104**, 175 (2003).
[6]E. R. Leite, E. C. Paris, F. M. Pontes, C. A. Paskocimas, E. Longo, F. Sensato, C. D. Pinheiro, J. A. Varela, P. S. Pizani, C. E. M. Campos, and F. Lanciotti, Jr., J. Mater. Sci. **38**, 1175 (2003).
[7]A. Zhang, M. Lü, S. Wang, G. Zhou, S. Wang, and Y. Zhou, J. Alloys Compd. **433**, L7 (2007).
[8]V. M. Longo, L. S. Cavalcante, A. T. de Figueiredo, L. P. S. Santos, E. Longo, J. A. Varela, J. R. Sambrano, C. A. Paskocimas, F. S. De Vicente, and A. C. Hernandes, Appl. Phys. Lett. **90**, 091906 (2007).
[9]A. Bergh, G. Craford, A. Duggal, and R. Haitz, Phys. Today **54**(12), 42 (2001).
[10]H. Y. Hwang, Nat. Mater. **4**, 803 (2005).
[11]D. Kan, T. Terashima, R. Kanda, A. Masuno, K. Tanaka, S. Chu, H. Kan, A. Ishizumi, Y. Kanemitsu, Y. Shimakawa, and M. Takano, Nat. Mater. **4**, 816 (2005).
[12]S. Yamanaka, T. Hamaguchi, T. Oyama, T. Matsuda, S.-I. Kobayashi, and K. Kurosaki, J. Alloys Compd. **359**, 1 (2003).
[13]A. Erb, E. Walker, and R. Flükiger, Physica C **245**, 245 (1995).
[14]R. Liang, D. A. Bonn, and W. N. Hardy, Physica C **304**, 105 (1998).
[15]K. C. Goretta, E. T. Park, R. E. Koritala, M. M. Cuber, E. A. Pascual, N. Chen, A. R. de Arellano-Lopez, and J. L. Routbort, Physica C **309**, 245 (1998).
[16]S. Tao and J. T. S. Irvine, J. Solid State Chem. **180**, 3493 (2007).
[17]S. Yamanaka, K. Kurosaki, T. Maekawa, T. Matsuda, S.-I. Kobayashi, and M. Uno, J. Nucl. Mater. **344**, 61 (2005).
[18]J. Alarcon, D. van der Voort, and G. Blasse, Mater. Res. Bull. **27**, 467 (1992).
[19]Z. Lu, Y. Tang, L. Chen, and Y. Li, J. Cryst. Growth **266**, 539 (2004).
[20]H. Zhou, Y. Mao, and S. S. Wong, J. Mater. Chem. **17**, 1707 (2007).
[21]J. Tsay and T. Fang, J. Am. Ceram. Soc. **82**, 1409 (1999).
[22]T. Salmi, E. Paatero, and P. Nyholm, Chem. Eng. Process. **43**, 1487 (2004).
[23]C. Lee, W. Yang, and R. G. Parr, Phys. Rev. B **37**, 785 (1988).
[24]A. D. Becke, J. Chem. Phys. **98**, 5648 (1993).
[25]V. Saunders, R. Dovesi, C. Roetti, R. Orlando, C. M. Zicovich-Wilson, N. M. Harrison, K. Doll, B. Civalleri, B. Bush, and P. L. M. D'Arco, CRYSTAL03 User's Manual (University of Torino, Torino, 2003).
[26]J. R. Sambrano, E. Orhan, M. F. C. Gurgel, A. B. Campos, M. S. Góes, C. O. Paiva-Santos, J. A. Varela, and E. Longo, Chem. Phys. Lett. **402**, 491 (2005).
[27]S. R. de Lázaro, P. R. de Lucena, J. R. Sambrano, P. S. Pizani, A. Beltrán, J. A. Varela, and E. Longo, Phys. Rev. B **75**, 144111 (2007).
[28]http://www.crystal.unito.it/Basis_Sets/Ptable.html
[29]http://www.tcm.phy.cam.ac.uk/mdt26/crystal.html
[30]T. J. B. Holland and S. A. T. Redfern, Miner. Mag. **61**, 65 (1997).
[31]J. A. Nelder and R. Mead, Comput. J. **7**, 308 (1965).
[32]S. de Lazaro, J. Milanez, A. T. de Figueiredo, V. M. Longo, V. R. Mastelaro, F. S. De Vicente, A. C. Hernandes, J. A. Varela, and E. Longo, Appl. Phys. Lett. **90**, 111904 (2007).
[33]R. C. Lima, J. W. M. Espinosa, M. F. C. Gurgel, E. C. Paris, E. R. Leite, M. R. Joya, P. S. Pizani, J. A. Varela, and E. Longo, J. Appl. Phys. **100**, 034917 (2006).
[34]I. A. Souza, M. F. C. Gurgel, L. P. S. Santos, M. S. Góes, S. Cava, M. Cilense, I. L. V. Rosa, C. O. Paiva-Santos, and E. Longo, Chem. Phys. **322**, 343 (2006).
[35]M. Anicete-Santos, L. S. Cavalcante, E. Orhan, E. C. Paris, L. G. P. Simões, M. R. Joya, I. L. V. Rosa, P. R. de Lucena, M. R. M. C. Santos, L. S. Santos-Júnior, P. S. Pizani, E. R. Leite, J. A. Varela, and E. Longo, Chem. Phys. **316**, 260 (2005).
[36]E. Orhan, F. M. Pontes, E. R. Leite, P. S. Pizani, J. A. Varela, and E. Longo, ChemPhysChem **6**, 1530 (2005).
[37]V. M. Longo, E. Orhan, L. S. Cavalcante, S. L. Porto, J. W. M. Espinosa, J. A. Varela, and E. Longo, Chem. Phys. **334**, 180 (2007).
[38]M. Anicete-Santos, E. Orhan, M. A. M. A. de Maurera, L. G. P. Simões, A. G. Souza, P. S. Pizani, E. R. Leite, J. A. Varela, J. Andrés, A. Beltrán, and E. Longo, Phys. Rev. B **75**, 165105 (2007).
[39]D. L. Wood and J. Tauc, Phys. Rev. B **5**, 3144 (1972).
[40]E. Orhan, J. A. Varela, A. Zenatti, M. F. C. Gurgel, F. M. Pontes, E. R. Leite, E. Longo, P. S. Pizani, A. Beltràn, and J. Andrès, Phys. Rev. B **71**, 085113 (2005).
[41]L. S. Cavalcante, M. F. C. Gurgel, A. Z. Simões, E. Longo, J. A. Varela, M. R. Joya, and P. S. Pizani, Appl. Phys. Lett. **90**, 011901 (2007).
[42]K. Vanheusden, W. L. Warren, C. H. Seager, D. R. Tallant, J. A. Voigt, and B. E. Gnade, J. Appl. Phys. **79**, 7983 (1996).
[43]P. H. Kasai, Phys. Rev. **130**, 989 (1963).
[44]M. Z. Z. Jin, J. Zhang, X. Guo, J. Yang, W. Li, X. Wang, and Z. Zhang, J. Mol. Catal. A: Chem. **217**, 203 (2004).
[45]J. Matta, J.-F. Lamonier, E. Abi-Aad, E. A. Zhilinskaya, and A. Aboukaïs, Phys. Chem. Chem. Phys. **1**, 4975 (1999).
[46]C. Lin, C. Zhang, and J. Lin, J. Phys. Chem. C **111**, 3300 (2007).
[47]E. Longo, E. Orhan, F. M. Pontes, C. D. Pinheiro, E. R. Leite, J. A. Varela, P. S. Pizani, T. M. Boschi, F. LanciottiJr., A. Beltrán, and J. Andrés, Phys. Rev. B **69**, 125115 (2004).
[48]M. Zampieri, S. R. Lazaro, C. A. Paskocimas, A. G. Ferreira, E. Longo, and J. A. Varela, J. Sol-Gel Sci. Technol. **37**, 9 (2006).

[49]P. R. de Lucena, E. R. Leite, F. M. Pontes, E. Longo, P. S. Pizani, and J. A. Varela, J. Solid State Chem. **179**, 3997 (2006).
[50]R. Leonelli and J. L. Brebner, Solid State Commun. **54**, 505 (1985).
[51]R. I. Eglitis, E. A. Kotomim, and G. Bostel, Eur. Phys. J. B **27**, 483 (2002).
[52]D. P. Volanti, L. S. Cavalcante, E. C. Paris, A. Z. Simões, D. Keyson, V. M. Longo, A. T. de Figueiredo, E. Longo, J. A. Varela, F. S. De Vicente, and A. C. Hernandes, Appl. Phys. Lett. **90**, 261913 (2007).